A CALCULATION METHOD FOR THE THREE-DIMENSIONAL BOUNDARY-LAYER EQUATIONS IN INTEGRAL FORM

Bilal Mughal* and Mark Drela†‡

Computational Aerospace Sciences Laboratory

Department of Aeronautics and Astronautics

Massachusetts Institute of Technology, Cambridge, MA 02139

Abstract

A new numerical method is developed to solve the three-dimensional boundary-layer equations, in integral form, on non-orthogonal grids. The finite-volume scheme employed eliminates the need to compute metric-gradient terms found in curvilinear-coordinate finite-difference methods. The integral method is based on two equations for momentum and one for kinetic energy with empirical equilibrium compressible turbulent-flow closure relations selectively extracted from the literature. Johnston's model is used for the crossflow. The non-linear discrete equations are solved simultaneously using the Newton-Raphson method along a row of cells and the solution is marched successively downstream. Along each row, cell residuals are distributed to nodes in a manner consistent with the local direction of characteristic lines. Results are computed for a well-known infinite swept wing case to evaluate empirical-closure accuracy, and for a finite swept wing case to demonstrate the full three-dimensional capability.

Nomenclature

A	crossflow parameter
$c_{D_{()}}$	coefficient of dissipation
$c_{f_{()}}$	skin friction
D	dissipation or shear-work integral
$E_{()()}$	components of $\theta^*_{()}$
F	flux vector
G	flux vector
$H_{()}$	shape factor
j	grid counter
$M_{()}$	Mach number
q	speed
R, $\tilde{R}$	vector of residuals
$Re_{()}$	Reynolds number
S	Source term vector
s, n	streamline coordinates
U	vector of primary variables
u, v, w	velocity components
x, y, z	Cartesian coordinates
α	generic angle
β	streamline angle w.r.t. to external flow
γ	characteristic line angle w.r.t. external flow
$\delta^*_{()}$	displacement thickness
$\delta^{**}_{()}$	density thickness
θ_ρ	auxiliary density thickness
$\theta_{()()}$	orientation-dependent momentum thickness
$\theta^*_{()}$	orientation-dependent kinetic-energy thickness
μ	laminar viscosity, residual distribution factor
ρ	density
τ	shear stress
$()_w$	value at wall
$()_e$	value at boundary-layer edge

*Graduate Research Assistant, Student Member AIAA

†Associate Professor, Member AIAA

1 Introduction

There have been astonishing advances, over the last several years, in the development of Navier-Stokes solvers capable of generating solutions over realistic aircraft configurations. The generation of each solution, however, requires considerable resources thus leaving these solvers outside the realm of routine design activities, especially those involving optimization. Coupled Euler/boundary-layer or Potential/boundary-layer methods, on the other hand, are far more economical; they have proved very useful in two dimensions and offer the same potential in three dimensions. Furthermore, difficulties in comprehensive modeling of turbulent flows puts Navier-Stokes solvers in the same league as these coupled methods in terms of solution accuracies. The present study is undertaken to model the boundary-layer part of a coupled solver.

An integral form of the equations is chosen over the usual differential form primarily because interest is largely confined to integral quantities. There is also an order of magnitude decrease in computational effort. Furthermore, integral schemes tend to be more robust and are better suited for viscous/inviscid calculations. On the other hand, an obvious disadvantage is the increased reliance on empiricism. In reality, however, integral methods have historically produced results of accuracy comparable to those generated by differential schemes [13].

The prediction of three-dimensional turbulent boundary-layer flows has only recently begun to garner attention, relative to two-dimensional flows, sufficient to match their ubiquitous presence in nature. One prominent reason is the sheer geometrical complexity of general extensions into a third dimension. The traditional finite-difference curvilinear formulation of the equations on non-orthogonal grids requires the evaluation of cumbersome metric and metric-gradient terms. This new method uses a finite-volume discretization approach to pose the computational problem in a simple locally-Cartesian form, without any additional metric-gradient terms.

A method of residual distribution is developed to account for the local flow-of-information directions in the system of hyperbolic equations. The resulting non-linear discrete equations are solved using the Newton-Raphson method.

2 Governing Equations

The steady compressible differential boundary-layer equations, in a Cartesian system, are integrated normal to the wall to obtain a system of three equations involving integral quantities (see, for example, [7]). In conservation form, they are:

$$\frac{\partial F}{\partial x} + \frac{\partial G}{\partial z} + S = 0\,, \tag{1}$$

where the flux vectors are

$$F = \begin{pmatrix} \rho_e q_e^2 \theta_{xx} \\ \rho_e q_e^2 \theta_{zx} \\ \rho_e q_e^3 \theta_x^* \end{pmatrix}$$

and

$$G = \begin{pmatrix} \rho_e q_e^2 \theta_{xz} \\ \rho_e q_e^2 \theta_{zz} \\ \rho_e q_e^3 \theta_z^* \end{pmatrix},$$

and the source vector is

$$S = \begin{pmatrix} \rho_e q_e \delta_x^* \partial u_e/\partial x + \rho_e q_e \delta_z^* \partial u_e/\partial z - \tau_{x_w} \\ \rho_e q_e \delta_x^* \partial w_e/\partial x + \rho_e q_e \delta_z^* \partial w_e/\partial z - \tau_{z_w} \\ \rho_e q_e \delta_x^{**} \partial q_e^2/\partial x + \rho_e q_e \delta_z^{**} \partial q_e^2/\partial z - 2D \end{pmatrix}.$$

The dissipation or shear-work integral D can be written as the sum of two components, one due to the wall-normal gradient of velocity in the x direction and the other due to the gradient in the z direction, such that

$$D = D_x + D_z\,.$$

The first two equations involve the momentum deficit and are simple 3D extensions of the 2D von Kármán equation while the last is a relation for shear work or kinetic-energy dissipation. These equations are valid in laminar and turbulent flow regimes; in turbulent flow, the variables are interpreted to be meanflow quantities.

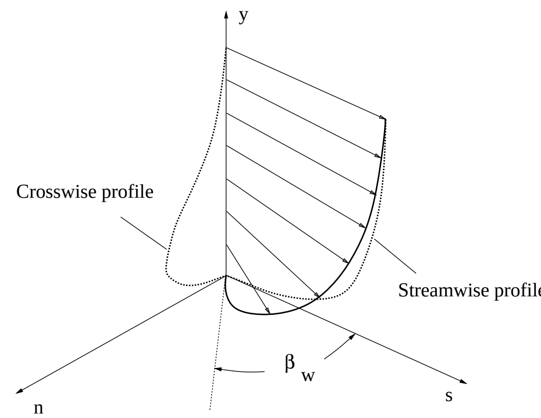

Figure 1: Velocity distribution in a typical 3D boundary layer

For the special case where the coordinates (x, z) are aligned with the coordinates (s, n), formed by the external flow streamline and crossflow directions respectively, numeric subscripts $(1, 2)$ are used instead of (x, z).

The components of the vector U are the three chosen primary unknowns,

$$U = \begin{pmatrix} \theta_{11} \\ \beta_w \\ \delta_1^* \end{pmatrix},$$

where β_w is the limiting streamline angle, as shown in Figure 1.

The three first-order integral equations are hyperbolic. The system can be diagonalized into decoupled equations involving the characteristics. Eigenvalues of the system are real and distinct and correspond to the the tangent of the angle that the characteristics make with the external flow streamline.

For an incompressible, turbulent system of momentum-integral and entrainment relations, Cousteix and Houdeville [3] show that one of the characteristic lines lies close to the limiting wall streamline. In Figure 2, this characteristic line is labeled γ_1. The other two characteristic lines always lie between the external-flow streamline and the limiting wall streamline. The calculation of reasonable characteristic directions, therefore, constitutes a demonstration of the validity of the closure employed.

3 Empirical relationships for closure

Empirical relations are necessary to make the problem determinate. All non-primary variables are correlated to the three primary unknowns, θ_{11}, δ_1^* and $\tan(\beta_w)$, using assumed forms of velocity profiles together with empirical

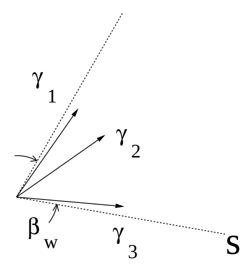

Figure 2: Characteristic directions in a 3D boundary layer

skin-friction and dissipation relations derived from experiment.

There isn't a substantial observed improvement in accuracy when using field methods instead of equilibrium ones in the equations [13]. Therefore, in the interests of simplicity, closure of the integral equations is achieved by equilibrium empirical models. These models are obtained from the literature.

The traditional methodology employed in three-dimensional closure has been to assume two-dimensional-like behavior of the boundary layer in the streamwise direction because there is a close experimental resemblance between three-dimensional streamwise profiles and two-dimensional boundary layers [8]. One fortunate outcome of this assumption is that empirical correlations of the streamwise variables in three-dimensional flows can draw a considerable amount of information from the better-explored two-dimensional flows. Clearly, this approach works best when the crossflow is small.

3.1 Streamwise Closure

Turbulent boundary layers have a two-layer structure where the thickness of each layer scales differently with $\overline{Re}_\theta$. Therefore, at least two independent parameters are needed to adequately describe a velocity profile. The analytical formula that is employed in this calculation method was developed by Swafford [11]. It is the sum of two independent transcendental functions, one expressed in terms of the inner variable $\bar{y}^+$ and the other expressed in terms of the outer variable $y/\bar{\theta}$.

Following the observation that the velocity distribution in the streamwise direction may be represented by profile families developed for two-dimensional flows, it has often been assumed that the streamwise component of skin friction may also be obtained by using skin-friction relations applicable to two-dimensional flows [8]. The presence of the law-of-the-wall as one component of the two-parameter family of profiles enables one to correlate $\bar{u}_e^+$ in terms of two integral parameters, for example H and $Re_{\theta_{11}}$, thereby yielding an expression for the streamwise component of skin friction. The relation employed in this calculation method was also developed by Swafford [11].

The assumption that the streamwise component of wall shear is related to the streamwise velocity profile implies that the law-of-the-wall applies to the velocity profile in its usual two dimensional form. Strictly, this is incorrect. This assumption is likely to be of more consequence, however, in methods employing differential equations while in integral methods, errors thus introduced are unlikely to be more serious than those originating from other sources [8].

A thickness, E_{11}, that depends only on the streamwise velocity in the boundary layer is defined such that

$$\rho_e q_e^3 E_{11} = \int_0^\delta \rho u (u_e^2 - u^2)\, dy \,.$$

This thickness is the streamwise component of θ_1^* and can be correlated to H and $Re_{\theta_{11}}$ through the streamwise velocity profile. The correlation employed is one due to Drela [5]. In addition to this relation, another proposed by Whitfield et. al. [14] was also considered. It produced results almost indistinguishable from those using Drela's equation. However, for one calculation (the van den Berg/Elsenaar infinite wing) it failed to yield characteristic directions coherent with the computed result in that one or more of these characteristic directions was significantly outside the range of the limiting and external-flow streamlines. The failure was presumably due to an assumption in their derivation that effectively eliminated the dependence on Reynolds number as noted by Drela [5]. Consequently, the sensitivity of the characteristic directions to the Jacobian-matrix elements involving $H_{E_{11}}$, especially at low Reynolds numbers, was probably erroneous. Drela's expression does not include this simplification.

The correlation for compressible density thickness employed is only a function of the shape parameter and Mach number and is given by Whitfield et. al. [14].

The coefficient of dissipation due to the surface-normal gradient of velocity in the streamwise direction was taken from Whitfield et. al. [14]. It was derived by numerically evaluating the dissipation integral using a constant laminar plus turbulent shear stress in the region very near the wall and an eddy-viscosity model in the inner and outer regions.

3.2 Crosswise Closure

The crossflow model employed in this calculation method is Johnston's hodographically triangular one [6]. In this model, within a thin layer adjacent to the surface, the crosswise velocity is related to the streamwise one by

$$\frac{w}{u} = \tan(\beta_w)\,.$$

Over the remaining portion of the boundary layer,

$$\frac{w}{q} = A\left[1 - \left(\frac{u}{q}\right)\right].$$

The parameter A is a measure of the crossflow magnitude and can be related to β_w. Smith [10] provides a relation,

$$A = -\tan(\beta_w)\left[\frac{\sqrt{c_{f_1}\cos(\beta_w)(1+0.18\,M_e^2)}}{0.10 - \sqrt{c_{f_1}\cos(\beta_w)(1+0.18\,M_e^2)}} - 1\right],$$

which includes the effects of compressibility.

While A appears explicitly instead of β_w in the crossflow variable relations, the latter is, nevertheless, chosen as a primary variable because it is uniquely related A. The reverse is not true.

The crossflow component of wall shear stress is related to the streamwise one through the limiting-streamline angle,

$$\tau_{z_w} = -\tan(\beta_w)\,\tau_{x_w}\,.$$

The dissipation coefficient due to the crossflow is expressed in terms of that due to the streamwise flow and the parameter A,

$$c_{D_2} = \frac{D_2}{\rho_e q_e^3} = \left(\frac{|A|}{14667\,c_{D_1} + 3.0}\right)^{\frac{|A|+10.0}{1020\,c_{D_1}+4.0}},$$

where $c_{D_1} = D_1/\rho_e q_e^3$. This correlation was derived by numerically evaluating the integral

$$\int_0^\delta |\tan(\beta)|\tau_1 \frac{\partial u}{\partial y}\,dy\,,$$

using Cebeci-Smith's two-layer eddy-viscosity model [1].

The remaining thickness variables can be readily related to the streamwise ones through the shape factors using the assumed shape of the crossflow velocity profile. As an example,

$$\theta_{21} = -A\,\theta_{11}\,.$$

Finally, the identity

$$\theta_{12} \equiv \theta_{21} - \delta_2^*$$

completes the determinancy of the system of equations and variables.

It is important to point out that these relationships were derived using only the outer portion of Johnston's model, which is equivalent to assuming that the profile $w(u)$ is linear in the hodograph plane. Obviously, the hypothesis of linearity is wrong near the wall because of the no-slip condition, but the concerned region is very thin. Cousteix and Houdeville [3] claim that the resulting error in the estimated thicknesses is negligible even if the maximum value of w occurs where u/q_e is approximately 0.6. Consequently, this approximation is expected to be valid and is unlikely to significantly affect the accuracy of the crossflow results.

4 Numerical Scheme

Discrete coupled equations are solved simultaneously for rows of cells, each considered individually, as part of space marching the solution along a direction corresponding approximately to the primary external-flow direction. The procedure involved in constructing the discrete equations requires the definition of global and local Cartesian coordinate systems.

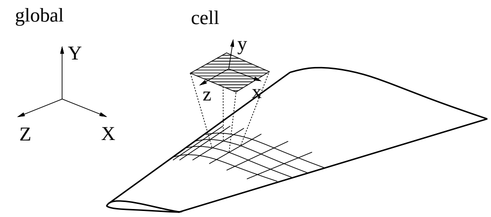

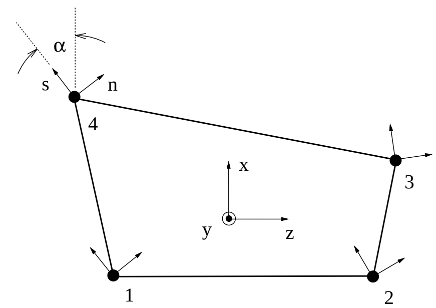

Figure 3: Global, cell and nodal streamline coordinate systems

4.1 Coordinate Systems

The basic computational element is a planar cell, individually constructed from body coordinates in the global Cartesian system. A local Cartesian coordinate system, denoted (x, z), is defined at the cell as illustrated in Figure 3. In the current formulation, this system is oriented so that the z-axis is parallel to face 1-2 of the the cell. The x-axis corresponds roughly to the external streamline direction and to the solution marching direction. A right-handed coordinate system will, therefore, correspond to the y-axis pointing out of the cell.

An additional local coordinate system, denoted by (s, n), is defined at each of the four nodes of the cell such that s is aligned to the external flow streamline direction and n to the crossflow direction. This is the discrete version of the analytic streamline system discussed earlier. It is necessary to define this system to accommodate the empirical relations discussed in the previous section.

Most variables are orientation dependent. Transformation relationships between the (s, n) and (x, y) coordinates are readily obtained by substituting the transformed velocity components $(\tilde{u}, \tilde{w})$,

$$\begin{pmatrix} \tilde{u} \\ \tilde{w} \end{pmatrix} = \begin{pmatrix} \cos(\alpha) & -\sin(\alpha) \\ \sin(\alpha) & \cos(\alpha) \end{pmatrix} \begin{pmatrix} u \\ w \end{pmatrix},$$

into variable definitions, where α is the angle between the coordinate directions s and x. For example, the two components of the displacement thickness in (x, y) are enough to uniquely determine the components in (s, n),

$$\delta_1^* = \cos(\alpha)\,\delta_x^* - \sin(\alpha)\,\delta_z^*$$

$$\delta_2^* = \sin(\alpha)\,\delta_x^* + \cos(\alpha)\,\delta_z^*$$

Rotation of all vector quantities into the local cell system before differencing properly accounts for the grid non-orthogonality. These transformations are effectively equivalent to adding the necessary metric-gradient terms that arise when the equations are written for a general curvilinear coordinate system.

4.2 Derivative Terms

The first-order derivative terms are discretized using Green's theorem by performing a discrete contour integral around a cell. The value at an edge of the cell is simply an average of the values at the two neighboring nodes. The discrete terms are formally second-order accurate.

4.3 Local Construction of Discrete Equations

The discrete equations along each row of cells are solved separately, as indicated earlier. For each of these rows, the constituent cells are visited individually, at each iteration, and a residual-vector, $\boldsymbol{R}$, is constructed for the cell. $\boldsymbol{R}$ is a function of the variables at the four nodes of the cell. The solution is stored at the nodes.

The vector of primary variables U is known at nodes 1 and 2 from the solution at the previous upstream row. The values at nodes 3 and 4 are unknown. They are initialized to be equal either to the values at nodes 1 and 2, respectively, or to the linear extrapolation of the values at nodes 1 and 2 and next upstream nodes. It is necessary that these initialized values be considered to be in the local (s, n) coordinate system.

The procedure employed at each of the nodes at a cell is as follows. First, the closure formulae are applied to determine all the non-primary unknowns as a function of U in the (s, n) system. Next, these unknowns are rotated into (x, z) coordinates. Then, in Equation 1 the derivative terms are approximated by the finite-volume method and the source term components by averaging the nodal values. The derivatives of velocities are also evaluated using the finite-volume method from their known components in the (x, z) system at the nodes and then simply multiplied to the remaining source-term cell-averaged variables.

The system of three discrete equations, thus developed, can be expressed as a function of the unknowns by writing the residual vector $\boldsymbol{R}$ as a function of U at the two downstream nodes 3 and 4, $\boldsymbol{R} = \boldsymbol{R}(U_3, U_4)$.

4.4 Boundary Conditions

An initial condition needs to be prescribed along the first row of nodes to start the calculation. Physically, fluid has to be entering the calculation domain along this initial row of cells to satisfy the characteristic direction requirement.

Along a row of N cells, there are 3N+3 primary unknowns but only 3N discrete equations. Therefore, three additional equations need to be supplied to determine the solution. These equations can be specified at the boundary nodes or at an interior node.

It is clear from the domain of influence principle that boundary conditions must be specified along those edges of the domain where characteristic directions indicate the passage of information into the domain. In principle, as many boundary conditions as there are characteristics crossing the boundary are required. An immediate corollary is that in regions where characteristics indicate that information is outbound, no conditions are needed; if any are applied, they will exert no influence on the solution in the interior of the domain. By the same reasoning, the effect of boundary conditions on the solution is limited to a region bounded by the path traced by the most angularly-directed characteristic.

For situations where Dirichlet conditions are not known at the domain boundary, zero-curvature boundary conditions, where the value at the boundary node is extrapolated from the two adjacent ones, are found to perform adequately. These are preferred over Neumann conditions where an arbitrary gradient is specified because the latter, in general, will not be consistent with the gradients of external velocity components and edge density.

4.5 Residual distribution to nodes

The directions of the characteristic lines have to be considered in the assembly of the system of cell residuals $\boldsymbol{R}$. This is achieved by defining a new vector of residuals $\tilde{\boldsymbol{R}}$ such that

$$\tilde{R}_j = (1 - \mu_k) R_j + \mu_k R_{j+1} \; ,$$

where μ_k is a function of the angle α that the local k^{th} characteristic makes with the corresponding cell edges. In Figure 4, which can be considered a scalar case, α is positive clockwise so that for the characteristic oriented towards the right in Figures 5 and 6, μ will be greater than 0.5. Thus, $\tilde{\boldsymbol{R}}$ corresponds to the net residual contributions at a node of the residual vectors of the two neighboring cells in proportion to the local direction of information flow. The slope of the μ function at $\alpha = 0$ is a user control.

In principle, the residual of the equation in terms of a characteristic variable should be distributed in proportion to the angle of the corresponding characteristic. In the current formulation, however, the distribution of the entire vector of residuals for the conservative formulation of Equation 1 is governed by the same value of μ. This is coupled to the γ_1 characteristic direction computed at the upstream row of nodes. While not ideal, this choice is found to perform satisfactorily in practice.

Two residual equations at either end of the row of cells are provided as boundary conditions. These will blend into the global system of equations when the γ_1 characteristic is inbound. In Figure 5, a "shock" is schematically illustrated;

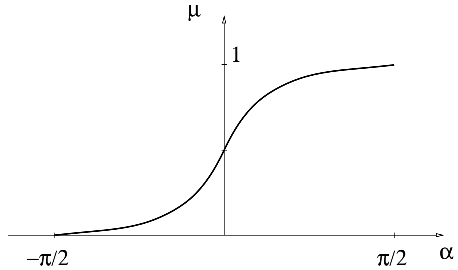

Figure 4: Residual distribution factor variation with angle

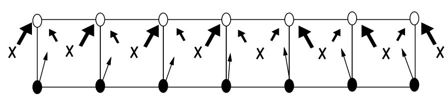

Figure 5: "Shock-cell" configuration

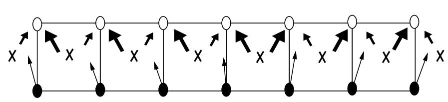

Figure 6: "Expansion-cell" configuration

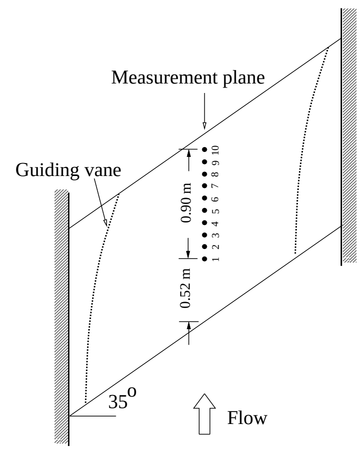

Figure 7: Schematic of van den Berg/Elsenaar experimental setup

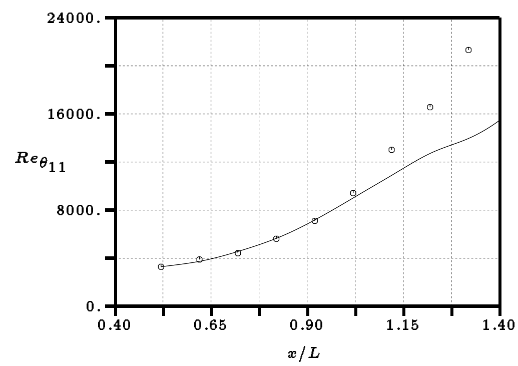

Figure 8: Computed variation of Reynolds number

the characteristic reverses direction in a manner where both boundary conditions are factored into the global system. In the limit that the slope of $\mu(\alpha)$ becomes infinite at $\alpha = 0$, this method is equivalent to discarding the residual equation at the shock cell. An "expansion" case is shown in Figure 6. Here, in the limit of infinite $d\alpha/d\mu(\alpha = 0)$, the global system becomes singular because the same residual is distributed to two nodes. Hence, one of the equations is replaced by an internal boundary condition which simply forces the variables at one of the two singular nodes to be the average of the values at the two adjacent nodes.

The set of coupled non-linear discrete equations, $R(U) = 0$, are solved using the well-known Newton-Raphson method. The Jacobian-matrix $[\partial R/\partial U]^m$ elements are constructed at the FORTRAN level by successive multiplication and addition of constituent partial derivatives using the chain rule. The global Jacobian-matrix structure is block-tridiagonal in the interior. For zero-curvature boundary conditions, the blocks in the next off-diagonal will be zero at one or both ends of the matrix.

5 Results

Some results from two calculations are presented in this section. The first was performed to simulate a quasi-two-dimensional flow. The primary intention was to compare the computed results with a well-known experiment in order to verify the empirical closure employed. The latter calculation was performed over a finite swept tapered wing mainly to demonstrate this method's three dimensional capabilities.

5.1 An Infinite Swept Wing

The experimental results presented here were obtained on an "infinite swept wing" under incompressible flow conditions. The experiment was conducted by van den Berg

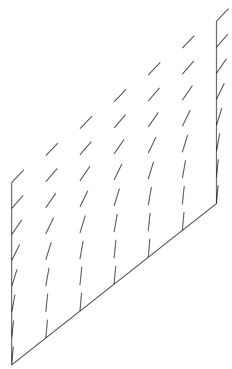

Figure 9: Computed limiting-streamline vector plot

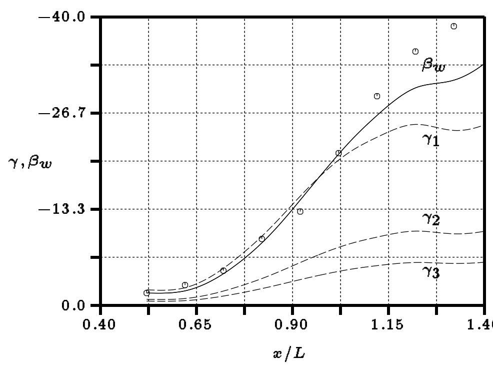

Figure 10: Computed variation of limiting-streamline and characteristic angles

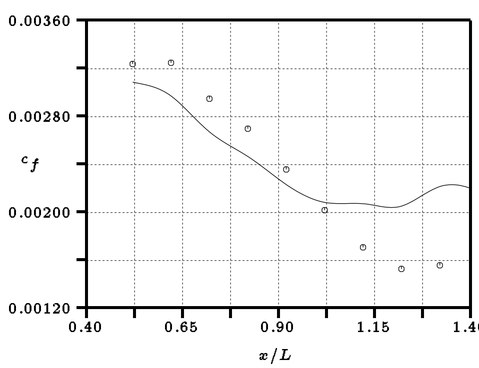

Figure 11: Computed variation of skin friction

and Elsenaar at The Netherland's National Aerospace Laboratory in 1972 [12].

The wing is actually a flat plate with an adverse pressure distribution induced on it by a suitably-shaped body positioned near the plate. The experiment was designed so that, over the forward portion of the experimental model, the pressure remained nearly constant before being made to increase gradually through the presence of the body. The pressure-gradient and sweep combine to induce three-dimensional separation in the vicinity of the trailing edge.

Considerable care was exercised in the attempt to simulate infinite-wing conditions. The boundary layer could be maintained very nearly quasi-two-dimensional with the help of guide vanes on either side of the region of interest. The positions of the measurement stations relevant to this calculation are depicted on the experimental model along with other notable features in Figure 7. The line of equally-spaced measurement stations was 0.90 m long. The angle of sweep of the wing was 35°.

Detailed measurements and descriptions of the experimental techniques are provided by the authors. This experiment has been extensively used to compare details of closure assumptions in many different kinds of numerical methods (see, for example, [3, 10, 13]).

The calculation was performed on a 200×3 grid assuming quasi-two-dimensional flow. One set of grid-lines was parallel to the freestream direction and the other to the wing leading edge. The computational domain corresponded to the region enclosed by stations 1 and 10 in the experiment.

A cubic spline-interpolation technique was employed to smooth the supplied external velocity measurements. Clearly, the spanwise component of velocity gradually increases downstream. The initial condition used was the set of experimentally-obtained values at the first station. A simple boundary condition was applied where zero-gradients were enforced in the direction of the wing isobars, and thus one set of grid lines, along the side of the computational domain with the inflow.

Computed results are presented in Figures 8 to 11 as the solid line. The marching coordinate has been scaled by a length of 1 m which is on the order of the wing chord.

The comparison for $Re_{\theta_{11}}$ is good up to the station near $x/L \approx 1.0$, where the spanwise flow is still a small fraction of the flow in the marching direction. This is also the case with the comparison for β_w. The negative value of β_w indicates that the limiting streamlines are turning spanwise faster than the external flow streamlines with marching distance. The tuft plot in Figure 9 vividly illustrates this turning. The calculated three-dimensional separation line occurs where the limiting streamlines coalesce and this is found to be close to the experimentally observed location. Experimentally, separation is observed between stations 8 and 9, or where $x/L \approx 1.3$. Figure 10 is a plot of the variation of the three calculated characteristic directions, shown in broken lines, juxtaposed against the solid line for β_w. The three characteristic lines are observed to be oriented largely within the angular limits defined by the external flow streamline (β_w, $\gamma = 0$) and the limiting wall

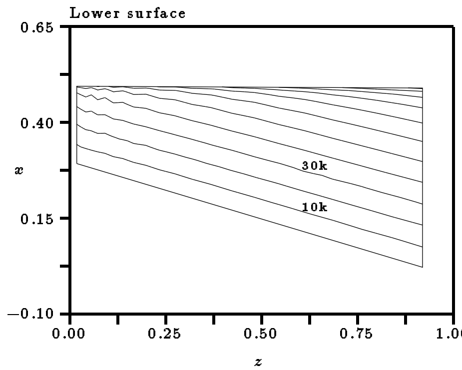

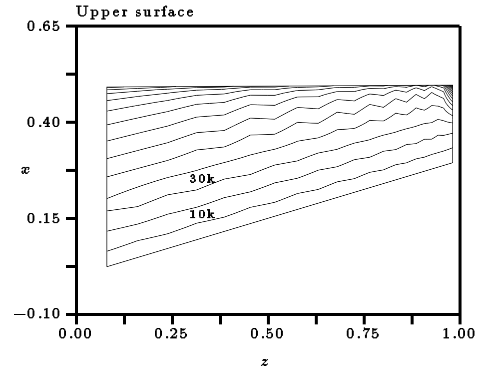

Figure 12: Computed Reynolds number contour plots

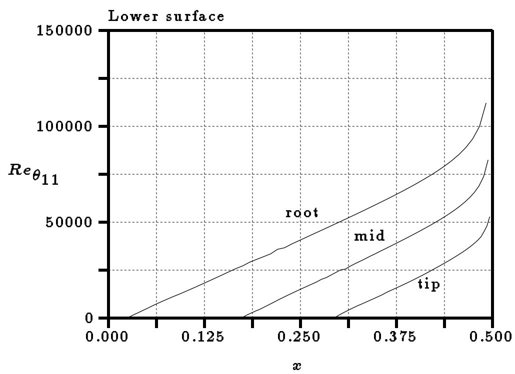

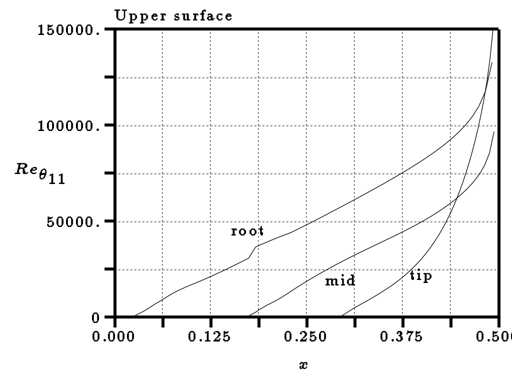

Figure 13: Computed Reynolds number chordwise variation

streamline. Furthermore, the line labeled γ_1 is evidently that associated with the limiting wall streamline.

The computed values of c_f and H compare less favorably with the experimental data. The trend of c_f closely follows that of other published numerical case studies, employing equilibrium closure, for the same experiment [10, 13]. Comparisons are good to $x/L \approx 1.0$ but almost universally poor beyond, providing strong evidence for the widely-acknowledged inadequacy of equilibrium closure in situations with separation and large crossflow.

5.2 A Finite Swept Tapered Wing

The development of a compressible boundary layer over a finite tapered swept wing, at the moderate angle of attack of 1.5° and a Mach number of 0.3, was calculated to demonstrate the full three-dimensional capabilities of this method. The wing section is a NACA 0012 airfoil. The external inviscid velocity and density distributions are supplied by a potential flow solver [9].

The wing-surface meshes measure 57×22 on both the upper and lower surfaces with the greater number of nodes in the chordwise direction. It is important to note that the global z-coordinate direction on the lower surface is opposite to that on the upper surface. This is necessitated by the convention that the y-coordinate increase in the direction, normal to the surface, on the side with the flow. All coordinates are normalized using the wingspan.

The external flow is nominally two-dimensional over most of the wing except in the leading edge and tip regions, where the spanwise components of velocity are significant.

The calculation is performed for a freestream Reynolds number, based on the mid-wing chord, Re_c, of 50×10^6. This is typical for a large transport in cruise where transition occurs at the attachment line.

The initial condition is estimated from the solution of the incompressible equations for laminar flow, using Falkner-Skan profiles, to generate a value for δ_1^* at the nodes on either side of the attachment line [2]. The assumption that the flow is locally identifiable with the flow on the leading edge of an equivalent infinite swept wing is made. In addition, a value of $H = 1.3$ is specified to yield the initial condition for θ_{11}. These thicknesses need to be scaled slightly to insure that $Re_{\theta_{11}}$ is within the range necessary to sustain turbulent flow and consequently also within the range of the empirical correlations. β_w is approximated to be zero. This process only requires $\partial u_e/\partial n$ at the attachment line and the laminar viscosity μ as inputs. While this approach is approximate it is nevertheless employed because the strong favorable pressure gradient which exists just downstream of the attachment line tend to make conditions over the major part of the wing comparatively insensitive to conditions on the attachment line [4].

Two sets of computed results, one each for $Re_{\theta_{11}}$ and β_w are shown in Figures 12 to 15. Each set consists of contour

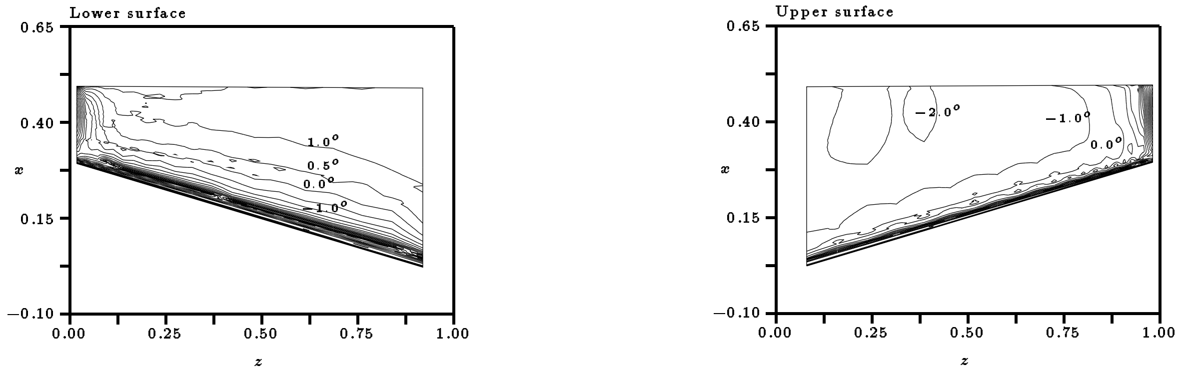

Figure 14: Computed limiting-streamline-angle contour plots

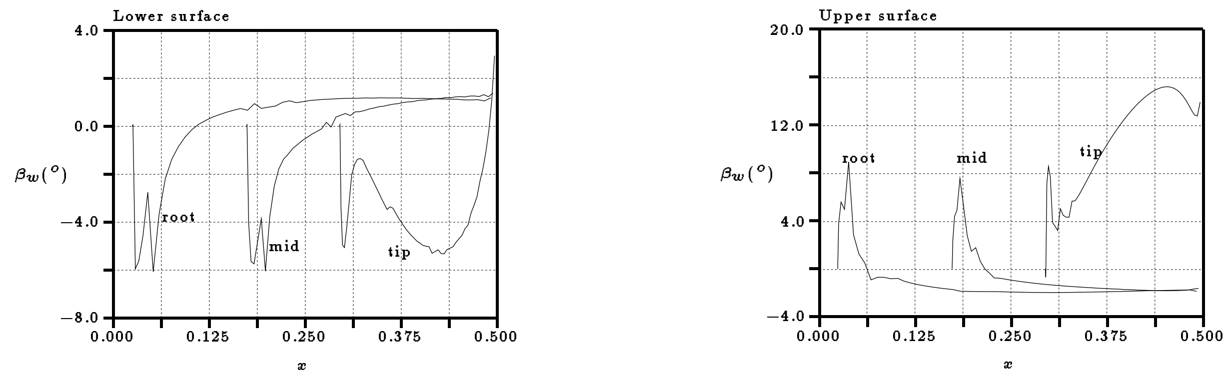

Figure 15: Computed limiting-streamline-angle chordwise variation

plots and line plots along three chordwise stations for both the upper and lower surfaces: the root, near midwing and at the tip. Note that counterclockwise angles are considered positive.

Unlike the infinite swept wing case where a sustained adverse pressure gradient was applied to induce three-dimensional separation, it is found here that, for the Re_c considered, the flow is attached over the entire wing surface.

The variation of β_w confirms that the most severe three-dimensional effects are largely restricted to areas near the leading edges and wing tips. Immediately downstream of the leading edge, drastic variations are seen. These are numerical effects, presumably a consequence of the slightly incorrect initial condition for β_w, the low values of $Re_{\theta_{11}}$ and the strong pressure gradient associated with the attachment line. However, the solution quickly becomes more placid with marching distance. As noted earlier these variations are not expected to have a substantial effect on the physical accuracy of the solution over the rest of the wing. Sawtooth oscillations seen in the contour plots are a result of numerical stiffness. A finer grid will alleviate the problem.

6 Concluding Remarks

A novel numerical method is developed for solving the three-dimensional integral boundary layer equations on non-orthogonal grids. The chief singular achievement of the method is the application of a finite-volume formulation that keeps the equations independent of surface and grid metrics. This results in substantial syntactic simplification and great flexibility in the choice of grids. In addition, a method of residual distribution from cells to nodes is developed to placate system hyperbolicity.

The use of an integral form of the equations yields a very fast method; the calculation on the finite wing takes only about 15 seconds on a DECstation 5000. In terms of integral variables, this method is as accurate as many differential, equilibrium-closure methods reported in a recent Eurovisc-Workshop [13].

The contextual basis of this paper is to develop a boundary layer method with the eventual aim of incorporating it into a viscous/inviscid code. The use of the Newton-Raphson technique is very helpful in this regard; the elements of the Jacobian-matrix can be appended to the global Jacobian matrix in a Newton-Raphson-based Full-Potential code to develop a global coupled scheme.

7 Acknowledgements

This research was supported by The Boeing Company under the supervision of Dr. Wen-Huei Jou.

References

[1] T. Cebeci and A. M. O. Smith. *Analysis of Turbulent Boundary Layers.* Academic Press, New York, 1974.

[2] J. Cousteix. Three-dimensional boundary layers. introduction to calculation methods. In *Computation of Three-Dimensional Boundary Layers Including Separation*, Apr 1986. AGARD-R-741.

[3] J. Cousteix and R. Houdeville. Singularities in three-dimensional turbulent boundary layer calcuations and separation phenomena. *AIAA Journal*, 19(8), Aug 1981.

[4] N.A. Cumpsty and M.R. Head. The calculation of three-dimensional turbulent boundary layers. part II: Attachment-line flow on an infinite swept wing. *The Aeronautical Quarterly*, 28:150–164, 1967.

[5] M. Drela. *Two-Dimensional Transonic Aerodynamic Design and Analysis Using the Euler Equations.* PhD thesis, MIT, December 1985. Also, MIT Gas Turbine & Plasma Dynamics Laboratory Report No. 187, Feb 1986.

[6] J.P. Johnston. *Three-dimensional turbulent boundary layers.* PhD thesis, MIT, 1957. Also, MIT Gas Turbine Laboratory Report No. 39.

[7] B. H. Mughal. A calculation method for the three-dimensional boundary-layer equations in integral form. Master's thesis, MIT, September 1992.

[8] J.F. Nash and V.C. Patel. *Three-Dimensional Turbulent Boundary Layers.* SBC Technical Books, Atlanta, 1972.

[9] P.B. Poll. Full potential analysis and design of transonic propellers. CFDL TR-91-1, MIT, Feb 1991.

[10] P. D. Smith. An integral prediction method for three-dimensional compressible turbulent boundary layers. R & M Report 3739, Aeronautical Research Council, HMSO, London, 1972.

[11] T. W. Swafford. Analytical approximation of two-dimensional separated turbulent boundary-layer velocity profiles. *AIAA Journal*, 21(6):923–926, 1983.

[12] B. van den Berg and A. Elsenaar. Measurements in a three-dimensional incompressible turbulent boundary layer in an adverse pressure gradient under infinite swept wing conditions. Technical Report NLR TR 72092U, Nationaal Lucht-En Ruimtevaartlaboratorium, Amsterdam, 1972.

[13] B. van den Berg, D.A. Humphreys, E. Krause, and J.P.F. Lindhout. Three-dimensional turbulent boundary layers – calculations and experiments. Notes on numerical fluid mechanics, Germany, 1988.

[14] D.L. Whitfield, T.W. Swafford, and T.L. Donegan. An inverse integral computational method for compressible turbulent boundary layers. In W. Haase, editor, *Recent Contributions to Fluid Mechanics.* Springer-Verlag, 1982.